Dirac semimetal films as spin conductors on topological substrates

Xiaoxiong Wang, Guang Bian, Peng Wang, and T.-C. Chiang

Phys. Rev. B **91**, 125103 — Published 2 March 2015

DOI: 10.1103/PhysRevB.91.125103

Dirac Semimetal Films as Spin Conductors on Topological Substrates

Xiaoxiong Wang[1*], Guang Bian[2,3], Peng Wang[4] and T.-C. Chiang[2,3*]

[1]College of Science, Nanjing University of Science and Technology, Nanjing 210094, China

[2]Department of Physics, University of Illinois at Urbana-Champaign, 1110 West Green Street, Urbana, Illinois 61801-3080, USA

[3]Frederick Seitz Materials Research Laboratory, University of Illinois at Urbana-Champaign, 104 South Goodwin Avenue, Urbana, Illinois 61801-2902, USA

[4]Department of Applied Physics, Shandong University of Science and Technology, Qingdao 266590, China

PACS numbers: 71.70.Ej, 73.20.At, 79.60.Dp, 73.40.-c

*e-mail: phywangxx@njust.edu.cn; tcchiang@illinois.edu

ABSTRACT

Spin-momentum locked states, notably those found on the surfaces of topological insulators, are promising for low-power electronic devices based on spin transport. Here we report a much more versatile case involving a Dirac semimetal film, theoretically modeled by low-Z substitution of Bi_2Se_3, on a Bi_2Se_3 topological insulator substrate. Such a film can carry highly spin-polarized conduction channels by electronic coupling to the substrate. The spin channel width, defined by the film thickness, is at the designer's disposal, thus permitting optimization of the system parameters. The results demonstrate Dirac semimetals as an important class of material for spintronic applications.

I. INTRODUCTION

A Dirac semimetal (DS) [1-4] exists at the phase boundary between a topological insulator (TI) [5-7] and a band insulator (BI). The prototypical TI Bi_2Se_3 [8, 9], for example, would be theoretically a BI without spin-orbit coupling (SOC), but it becomes a TI as the strength of the SOC is increased to its natural value [10]. At the critical point of the BI-TI phase transition, the singular DS phase exhibits a three-dimensional Dirac cone, and the valence and conduction bands meet at the Dirac point. This quantum critical point also marks the onset, under increasing SOC strength, of topological surface states within the inverted band gap opened up by the splitting of the Dirac cone into separate conduction and valance band continuums [11]. The topological surface states, being strongly spin polarized, have attracted much interest [12-14]. They are protected by the topological order (or time-reversal symmetry) [15, 16], but this protection also places a strong limit on opportunities for property modification and further optimization. The aim of our theoretical study is to design a system with enhanced properties and flexibility in tailoring the spin-conduction channels.

The specific case of interest is Bi_2Se_3 as a TI substrate and a low-Z substitute of the same material that forms a DS as a thin film overlayer. We find that the DS film by itself exhibits no useful spin texture, but it becomes a highly spin-polarized conductor upon contact with the TI substrate through a spin-bias interaction. For simplicity, low-Z substitution is modeled in our study by scaling the SOC strength in Bi_2Se_3 ranging from 0 to 100%. The lattice constant of the overlayer is fixed at the Bi_2Se_3 value, which corresponds to ideal epitaxial growth with no

relaxation. Experimentally, low Z substitution can be realized by replacing Bi in Bi_2Se_3 with Sb, for example, and Sb_2Se_3 is known to be a BI [8]. Our theoretical modeling of varying the SOC is only an approximation, but useful for illustrating the essential physics. Previous studies have shown that Bi_2Se_3 becomes a DS when its SOC strength is reduced to 31.2% of its natural value. Below this value, there are no surface states within the normal gap. Above this value, topological surface states exist to span the inverted gap. At the critical point, the topological surface states and the bulk band edge states become the same [10]. These "critical Dirac states" have unusual properties because of their simultaneous bulk and surface inheritance: their wave functions are bulklike, but their spin properties are very sensitive to the boundary conditions and can be readily spin biased. This is the key to building up the spin conduction channels.

II. COMPUTATIONAL METHODS

The calculation was performed with the ABINIT [17, 18] formulation using a plane wave expansion. The valence-nuclear interaction was described within the LDA approximation based on the Teter–Pade parameterization. The SOC was taken into account by adopting the Hartwigsen-Goedecker-Hutter (HGH) non-local pseudopotential [19]. It was scaled from 0 to 100% to simulate low-Z substitution. Momentum space sampling was carried on an $8\times8\times1$ grid. The cutoff of kinetic energy was 400 eV. It has been verified that a thickness of 6 QL for the substrate is sufficiently large to decouple its two faces with a negligible tunneling gap [20, 21]. Our calculations are based on a superlattice geometry with a vacuum gap of 20 Å between slabs.

III. RESULTS AND DISCUSSION

For notational simplicity, we refer to Bi_2Se_3 with a reduced SOC as $(Bi_2Se_3)'$. Each slab in the superlattice consists of 6 quintuple layers (QLs) of Bi_2Se_3 as the substrate, and 3 QLs of $(Bi_2Se_3)'$ on each side of the substrate as the overlayer [referred to as the 3/6/3 configuration as shown in Fig. 1(a)]; other superlattice configurations have also been analyzed. The calculated band structures of the 3/6/3 configuration are shown in Figs. 1(b)-1(e) for SOC = 0, 31.2, 50, and 100%, respectively. The subbands are color coded to show the surface weighted charge density; the results simulate what might be observed by angle-resolved photoemission – a surface sensitive technique [22, 23]. The corresponding spin-resolved planar change densities, defined by

$$\rho^{\pm}(k_x, z) = \iint \sum_i \left| \langle \pm | \psi_i(k_x, \mathbf{r}) \rangle \right|^2 dxdy , \qquad (1)$$

where $|\psi_i(k_x, \mathbf{r})\rangle$ is the state at k_x of the i-th band, $|\pm\rangle$ denotes the eigenstates of σ_y, and the summation is over each pair of spin degenerate states, are shown in the right panels [Figs. 1(f)-1(i)] for state A near the Dirac point with $k_x = \bar{\Gamma}\bar{\mathrm{M}}/40$. This value of k_x is chosen to be sufficiently small to be representative of the behavior around the zone center; it is nonzero to avoid the degeneracy at the zone center. The vertical dashed and solid lines indicate the boundaries of the QLs and the central substrate, respectively. Red and blue curves indicated the two opposite spin polarization directions along $\pm y$. The summation in Eq. (1) is taken over each Kramers pair. The case with SOC = 100% [Figs. 1(e) and 1(i)] correspond to a single 12-QL slab of Bi_2Se_3. The band structure shows the familiar topological surface states within the bulk gap.

The planar charge density for topological surface state A shows a spin separation at the two faces of the slab. The charge density distribution is mostly confined within the first QL near each face, and the net spin polarization at each face is about 70%. Note that state A actually sits below the valence band maximum along the $\bar{\Gamma}\bar{M}$ direction. As a result of the energy degeneracy with bulk bands which can act as electrical shorts, states near A are not particularly suited for device applications.

At SOC = 0% for the 3/6/3 configuration [Figs. 1(b) and 1(f)], the Bi_2Se_3 slab is sandwiched by BI slabs. State A gets lifted up into the bulk band gap and overlaps with no other bands in energy. The charge distribution is broad but peaks at the interfaces, which is characteristic of a BI/TI interfacial topological state [9]. As for the surface states in pure Bi_2Se_3, there is a pronounced spin separation [21]. The dispersion relations, however, show a wiggle at the Dirac point, resulting in a blunt Dirac cone, a reduced group velocity, and a reduced spin current.

The optimum case is achieved at SOC = 31.2% [Figs. 1(c) and 1(g)], where state A becomes nearly ideal spin conduction channels in the $(Bi_2Se_3)'$ overlayers: the probability density is nearly uniformly distributed within the overlayers; the spin polarization, almost 100%, is greater than that of the pristine topological surface state; the dispersion relations show a very steep Dirac cone with a high group velocity; and the Dirac point is well isolated in energy from the other bands, sitting about midway in an absolute gap of about 0.3 eV [8]. This gap is substantially larger than the thermal energy of 0.026 eV at room temperature, suggesting that

device operation at room temperature is feasible. The case of SOC = 50% [Figs. 1(d) and 1(h)] is similar to the 100% case, except that state A has a longer decay length toward the center of the slab. The trend in going from SOC = 0% to 100% is clear. State A changes from being interface-like to "bulk-like" to surface-like with a continuous shift of the spin/charge density. The bulk-like distribution occurs at the critical point. This trend is even more pronounced with thicker overlayers. An example is presented in Fig. 2, where the BI (SOC = 0%) overlayer thickness is doubled to 6 QL; state A, being an interface topological state, clearly decays away from the BI/TI interface. The states shown in Figs. 1(g) and 3(h) appear to be somewhat skewed within the DS films because of the asymmetric boundary conditions.

The projected bulk band structure of the DS phase at the critical SOC = 31.2% [Fig. 3(a)] shows a three-dimensional Dirac cone formed by the boundaries of the conduction and valance bands. The wave functions of states A and B are bulk-like [Fig. 3(e)]. The bulk bands reduce to sparse quantum well states in thin films. A 3-QL freestanding DS film [Fig. 3(b)] reveals a fairly large gap at the zone center because of the quantization. State A's charge distribution shows a slight spin bias [Fig. 3(f)], but the net spin within the film is zero; so this state is not suitable for spin transport. The case of a freestanding 6-QL film shows a similar behavior [Figs. 3(c) and 3(g)]. The same 6-QL DS films, made into a 6/6/6 configuration, support instead strongly spin-polarized state A [Figs. 3(d) and 3(h)]. These results confirm that freestanding DS films by themselves do not support spin conduction channels, but do so after they are made in contact with a TI substrate by spin separation across the TI substrate film. This phenomenon is mandated

by the topological order of the TI, which must carry boundary states with opposite spins on its two opposing faces [24, 25].

For a very thick film, or the bulk limit, the critical Dirac states in the DS phase [Fig. 3(a)] are at the bulk conduction and valence band boundaries. These states are delocalized and show no net spin in each QL [Fig. 3(e)] because of inversion symmetry. A slight increase of the SOC above the critical value separates these states from the bulk bands to become topological surface states characterized by spin separation toward the two faces of the system [10]. Yet these states must also remain almost bulk-like with a very long decay length. Evidently, it would cost very little energy in the bulk to spatially separate the spin at this juncture; the boundary condition then takes over as the dominant effect in deciding what spin configuration that the system should adopt. If the DS film is in contact with a TI, the overall topological order for the composite system mandates that the boundary states must be spin polarized. The very long or infinite decay length in the DS for these states means that the resulting spin conduction channel can effectively span the entire thickness of the DS film. While our calculations are for a symmetric sandwich configuration for simplicity (also to avoid unphysical vacuum dipole fields in asymmetric superlattices), each TI/DS interface is essentially isolated because of the large thickness of the TI substrate [20, 21]. For an asymmetric configuration, such as DS/TI/Vac, the DS/TI interface should behave similarly as long as the TI substrate is thick enough.

The topological states in a $(Bi_2Se_3)'$ overlayer on a Bi_2Se_3 substrate can be broadly classed into three regimes, as indicated schematically in Fig. 4. If the SOC of $(Bi_2Se_3)'$ is subcritical (BI

phase), the topological states are interface states confined at the BI/TI interface [Fig. 4(a)] [9]. If the SOC is overcritical (TI phase), the topological states are surface states with a distribution peaked at the surface of the composite system [Fig. 4(c)]. If the SOC is critical (DS phase), the topological states become overlayer states that span the DS film [Fig. 4(b)]. The three cases correspond to a normal gap, zero gap, and inverted gap in the overlayer material, respectively.

IV. CONCLUDING REMARKS

Spin conduction channels in DS films, arising from spin bias by a TI substrate and global topological order, offer excellent opportunities for spintronic applications [26-28]. Unlike the pristine topological insulator surface states, the overlayer topological states in DS films have an adjustable channel thickness that can be tailored for a higher current carrying capacity and other properties. Their spin polarizations, almost 100%, are better suited for signal processing. As illustrated by the comparison of 3-QL and 6-QL DS overlayers [Figs. 1(c) and 3(d)], the dispersion relations of the topological overlayer states are largely independent of the film thickness, and so variations in film thickness, which is a common problem in film preparation, does not appear to be an issue. Steps on surfaces are generally unavoidable. For Bi_2Se_3, QL steps are common [29], which can effectively decouple the topological states on neighboring terraces. This problem is minimized in DS overlayers with thicknesses of a few QLs or more. Our findings suggest an interesting avenue for applications of DS materials.

ACKNOWLEDGMENTS

This work was supported by the National Natural Science Foundation of China (No. 11204133 for XW), the Jiangsu Province Natural Science Foundation of China (No. BK2012393 for XW), the Young Scholar Project of Nanjing University of Science and Technology (XW), the US Department of Energy, Office of Science (Grant DE-FG02-07ER46383 for TCC), the Scientific Research Foundation of Shandong University of Science and Technology for Recruited Talents (No. 2013RCJJ024 for PW).

REFERENCES

[1] S. Young, S. Zaheer, J. Teo, C. Kane, E. Mele, and A. Rappe, Phys. Rev. Lett. **108**, 140405 (2012).

[2] Z. Wang, Y. Sun, X.-Q. Chen, C. Franchini, G. Xu, H. Weng, X. Dai, and Z. Fang, Phys. Rev. B **85**, 195320 (2012).

[3] Z. K. Liu, B. Zhou, Y. Zhang, Z. J. Wang, H. M. Weng, D. Prabhakaran, S. K. Mo, Z. X. Shen, Z. Fang, X. Dai, Z. Hussain, and Y. L. Chen, Science **343**, 864 (2014).

[4] Z. K. Liu, J. Jiang, B. Zhou, Z. J. Wang, Y. Zhang, H. M. Weng, D. Prabhakaran, S.-K. Mo, H. Peng, P. Dudin, T. Kim, M. Hoesch, Z. Fang, X. Dai, Z. X. Shen, D. L. Feng, Z. Hussain, and Y. L. Chen, Nat. Mater. **13**, 677 (2014).

[5] M. Z. Hasan and C. L. Kane, Rev. Mod. Phys. **82**, 3045 (2010).

[6] X.-L. Qi and S.-C. Zhang, Rev. Mod. Phys. **83**, 1057 (2011).

[7] D. Hsieh, D. Qian, L. Wray, Y. Xia, Y. S. Hor, R. J. Cava, and M. Z. Hasan, Nature **452**, 970 (2008).

[8] H. Zhang, C. X. Liu, X. L. Qi, X. Dai, Z. Fang, and S. C. Zhang, Nat. Phys. **5**, 438 (2009).

[9] W. Zhang, R. Yu, H. J. Zhang, X. Dai, and Z. Fang, New J. Phys. **12**, 065013 (2010).

[10] G. Bian, T. Miller, and T.-C. Chiang, Europhys. Lett. **101**, 27004 (2013).

[11] S. Souma, M. Komatsu, M. Nomura, T. Sato, A. Takayama, T. Takahashi, K. Eto, K. Segawa, and Y. Ando, Phys. Rev. Lett. **109**, 186804 (2012).

[12] P. Roushan, J. Seo, C. V. Parker, Y. S. Hor, D. Hsieh, D. Qian, A. Richardella, M. Z. Hasan,

R. J. Cava, and A. Yazdani, Nature **460**, 1106 (2009).

[13] Z. Wang, Y. Chong, J. D. Joannopoulos, and M. Soljačić, Nature **461**, 772 (2009).

[14] S. Kim, S. Yoshizawa, Y. Ishida, K. Eto, K. Segawa, Y. Ando, S. Shin, and F. Komori, Phys. Rev. Lett. **112**, 136802 (2014).

[15] C. L. Kane and E. J. Mele, Phys. Rev. Lett. **95**, 146802 (2005).

[16] L. Fu, C. L. Kane, and E. J. Mele, Phys. Rev. Lett. **98**, 106803 (2007).

[17] X. Gonze, G.-M. Rignanese, M. Verstraete, J.-M. Beuken, Y. Pouillon, R. Caracas, F. Jollet, M. Torrent, G. Zerah, M. Mikami, P. Ghosez, M. Veithen, J.-Y. Raty, V. Olevano, F. Bruneval, L. Reining, R. Godby, G. Onida, D. R. Hamann, and D. C. Allan, Z. Kristallogr. **220**, 558 (2005).

[18] X. Gonze, B. Amadon, P.-M. Anglade, J.-M. Beuken, F. Bottin, P. Boulanger, F. Bruneval, D. Caliste, R. Caracas, M. Côté, T. Deutsch, L. Genovese, P. Ghosez, M. Giantomassi, S. Goedecker, D. R. Hamann, P. Hermet, F. Jollet, G. Jomard, S. Leroux, M. Mancini, S. Mazevet, M. J. T. Oliveir, G. Onida, Y. Pouillon, T. Rangel, G.-M. Rignanese, D. Sangalli, R. Shaltaf, M. Torrent, M. J. Verstraete, G. Zerah, and J. W. Zwanziger, Comput. Phys. Commun. **180**, 2582 (2009).

[19] C. Hartwigsen, S. Goedecker, and J. Hutter, Phys. Rev. B **58**, 3641 (1998).

[20] Y. Zhang, K. He, C.-Z. Chang, C.-L. Song, L.-L. Wang, X. Chen, J.-F. Jia, Z. Fang, X. Dai, W.-Y. Shan, S.-Q. Shen, Q. Niu, X.-L. Qi, S.-C. Zhang, X.-C. Ma, and Q.-K. Xue, Nat. Phys. **6**, 584 (2010).

[21] O. V. Yazyev, J. E. Moore, and S. G. Louie, Phys. Rev. Lett. **105**, 266806 (2010).

[22] D. Lu, I. M. Vishik, M. Yi, Y. Chen, R. G. Moore, and Z.-X. Shen, Annu. Rev. Condens. Matter Phys. **3**, 129 (2012).

[23] Y. Chen, Frontiers of Physics **7**, 175 (2011).

[24] D. Hsieh, Y. Xia, D. Qian, L. Wray, J. Dil, F. Meier, J. Osterwalder, L. Patthey, J. Checkelsky, and N. Ong, Nature **460**, 1101 (2009).

[25] D. Hsieh, Y. Xia, L. Wray, D. Qian, A. Pal, J. Dil, J. Osterwalder, F. Meier, G. Bihlmayer, C. Kane, Y. S. Hor, R. J. Cava, and M. Z. Hasan, Science **323**, 919 (2009).

[26] I. Žutić, J. Fabian, and S. D. Sarma, Rev. Mod. Phys. **76**, 323 (2010).

[27] D. Pesin and A. H. MacDonald, Nat. Mater. **11**, 409 (2012).

[28] T. Yokoyama and S. Murakami, Physica E **55**, 1 (2014).

[29] H. Lin, T. Das, Y. Okada, M. C. Boyer, W. D. Wise, M. Tomasik, B. Zhen, E. W. Hudson, W. Zhou, V. Madhavan, C.-Y. Ren, H. Ikuta, and A. Bansil, Nano Lett. **13**, 1915 (2013).

FIG. 1 (color online). Electronic structure of Bi_2Se_3-$(Bi_2Se_3)'$ hetero-films with various SOCs. (a) Model of a superlattice unit cell made of a 6-QL Bi_2Se_3 slab as the substrate and a 3-QL $(Bi_2Se_3)'$ slab on each side as an overlayer. (b)-(e) Calculated band structure and simulated photoemission spectra for SOC = 0, 31.2, 50, and 100%, respectively, for the $(Bi_2Se_3)'$ layers. (f)-(i) Corresponding spin-resolved charge densities for the four cases (arbitrary normalization). Red and blue curves indicate the charge densities with spin polarization along $+y$ and $-y$, respectively. The vertical dashed and solid lines indicate the QL and substrate boundaries, respectively.

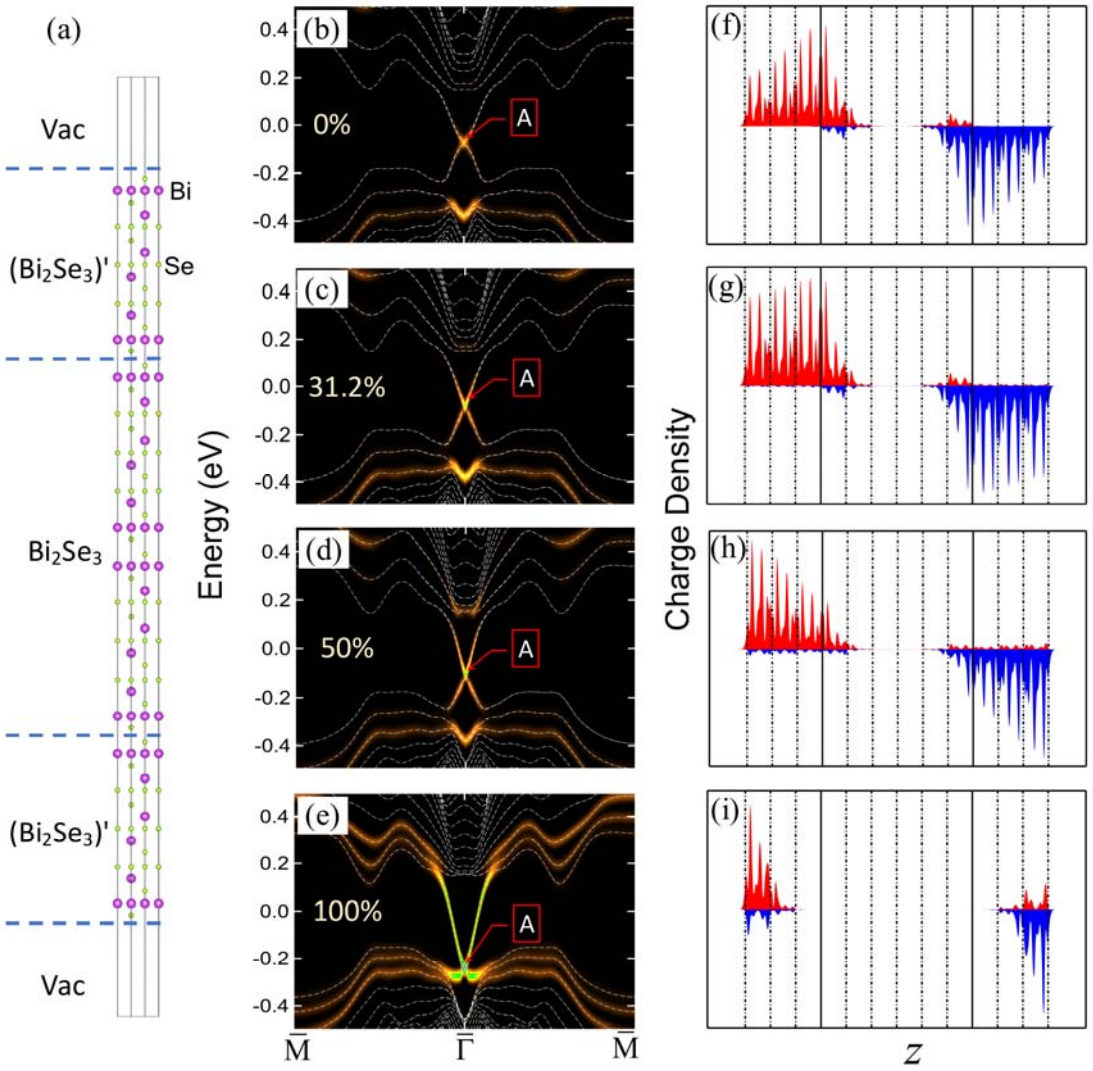

FIG. 2 (color online). Effects of changing the overlayer thickness for a BI/TI interface. (a) Band structure of a 6-QL Bi_2Se_3 slab sandwiched by 3-QL $(Bi_2Se_3)'$ (SOC = 0) slabs on both faces. (b) Spin resolved charge distribution of state A. (c) Same as (a) except that the $(Bi_2Se_3)'$ overlayer thickness is doubled to 6 QLs. (d) The spin-resolved charge distribution corresponding to (c). Evidently, state A is a topological interface state, which decays away from the interface.

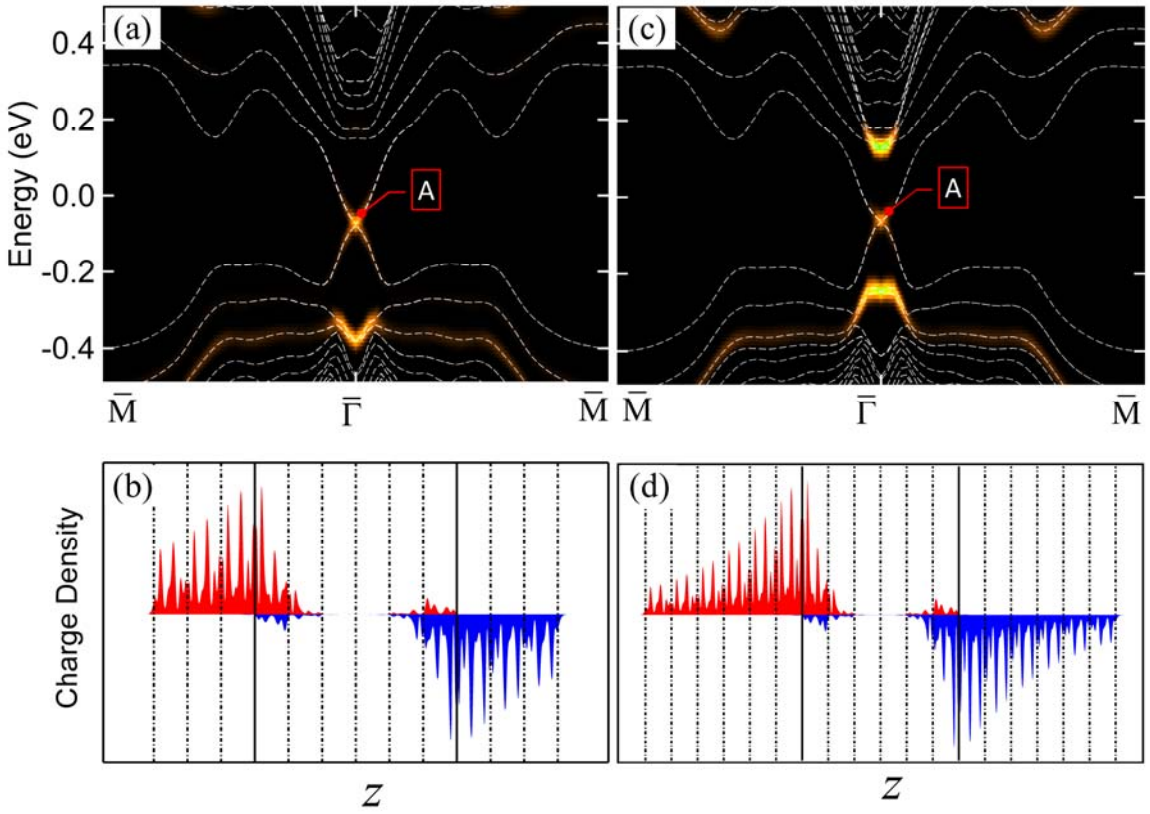

FIG. 3 (color online). Comparison of the electronic structures of DS bulk, films, and a DS-covered TI film. (a) Projected bulk band structure of $(Bi_2Se_3)'$ with SOC=31.2%. (b) Band structure of 3 QLs with SOC=31.2%. (c) Band structure of 6 QLs with SOC=31.2%. (d) Band structure of 6-QL Bi_2Se_3 sandwiched by 6-QL $(Bi_2Se_3)'$ (SOC=31.2%) on both faces. (e)-(h) Spin-resolved charge density of the states as indicated. The vertical dashed and solid lines indicate the QL and substrate boundaries, respectively.

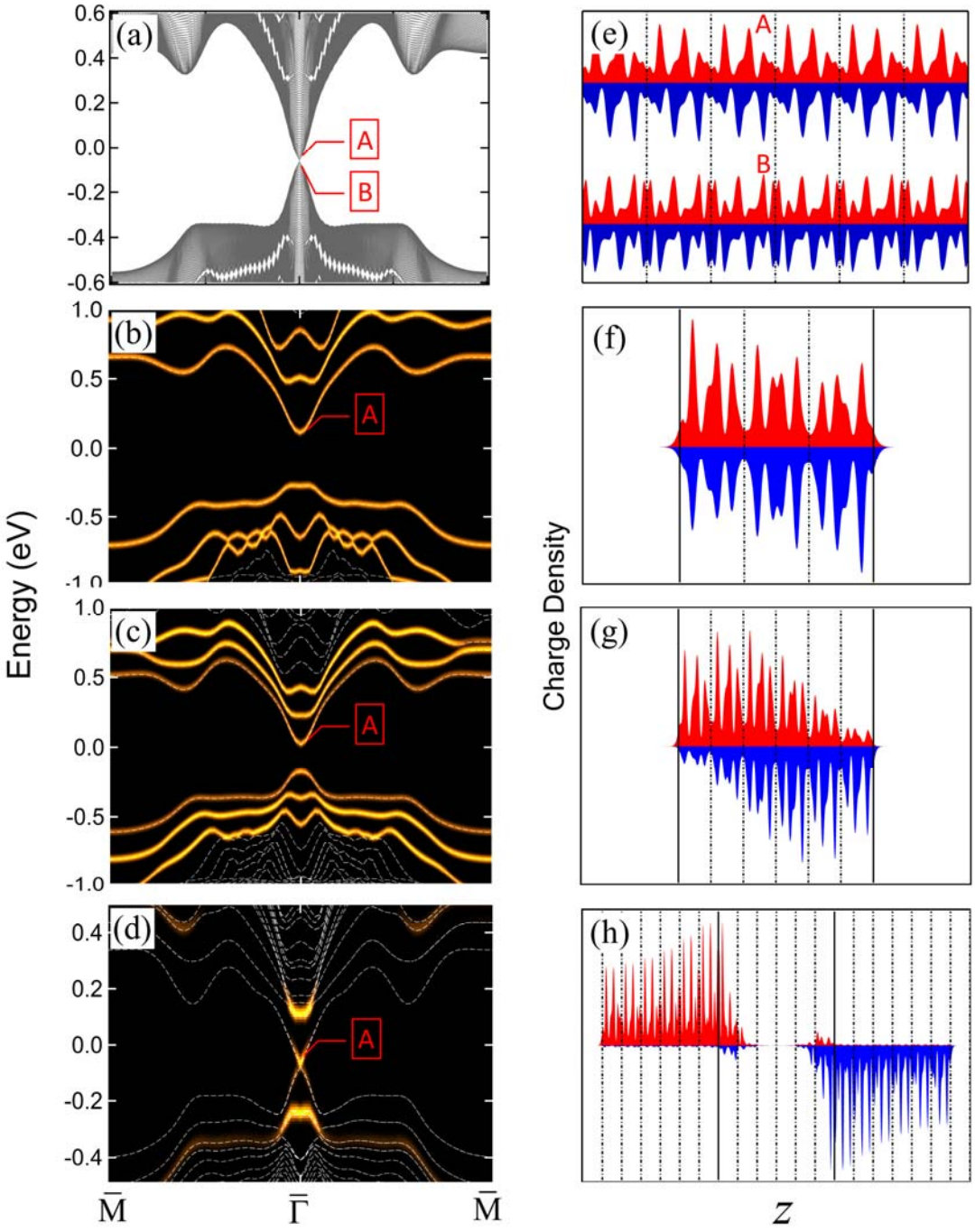

FIG. 4 (color online). Schematic charge distribution of the topological state for a Bi_2Se_3 substrate and a $(Bi_2Se_3)'$ overlayer. The three cases (a)-(c) correspond to the SOC of the $(Bi_2Se_3)'$ overlayer less than, equal to, and greater than the critical value, respectively, and so the overlayer is in the BI, DS, and TI phases. The solid horizontal lines indicate the position of the bulk band edge relative to the Dirac point in each case. The charge distribution corresponds to an interface, overlayer, and surface state, respectively.